Uniform phases in fluids of hard isosceles triangles: One-component fluid and binary mixtures

Yuri Martínez-Ratón* and Ariel Díaz-De Armas†
Grupo Interdisciplinar de Sistemas Complejos (GISC), Departamento de Matemáticas, Escuela Politécnica Superior, Universidad Carlos III de Madrid, Avenida de la Universidad 30, E-28911, Leganés, Madrid, Spain

Enrique Velasco‡
Departamento de Física Teórica de la Materia Condensada, Instituto de Física de la Materia Condensada (IFIMAC) and Instituto de Ciencia de Materiales Nicolás Cabrera, Universidad Autónoma de Madrid, E-28049, Spain

(Received 7 March 2018; published 11 May 2018)

We formulate the scaled particle theory for a general mixture of hard isosceles triangles and calculate different phase diagrams for the one-component fluid and for certain binary mixtures. The fluid of hard triangles exhibits a complex phase behavior: (i) the presence of a triatic phase with sixfold symmetry, (ii) the isotropic-uniaxial nematic transition is of first order for certain ranges of aspect ratios, and (iii) the one-component system exhibits nematic-nematic transitions ending in critical points. We found the triatic phase to be stable not only for equilateral triangles but also for triangles of similar aspect ratios. We focus the study of binary mixtures on the case of symmetric mixtures: equal particle areas with aspect ratios (κ_i) symmetric with respect to the equilateral one, $\kappa_1\kappa_2 = 3$. For these mixtures we found, aside from first-order isotropic-nematic and nematic-nematic transitions (the latter ending in a critical point): (i) a region of triatic phase stability even for mixtures made of particles that do not form this phase at the one-component limit, and (ii) the presence of a Landau point at which two triatic-nematic first-order transitions and a nematic-nematic demixing transition coalesce. This phase behavior is analogous to that of a symmetric three-dimensional mixture of rods and plates.

DOI: 10.1103/PhysRevE.97.052703

I. INTRODUCTION

Two-dimensional fluids of hard anisotropic particles are paradigms of systems where liquid-crystal (LC) phases can be stabilized solely by entropy. Hard-rod particles such as hard rectangles (HR), discorectangles (HDR), or ellipses (HE) exhibit the completely disordered isotropic (I) phase, but also a nematic (N) phase at higher densities where particle axes point, on average, along a common director. In two dimensions (2D) the N phase does not possess true long-range orientational order, and the N-I transition is usually continuous via a Kosterlitz-Thouless disclination unbinding mechanism. The N phase is stable for high enough aspect ratios, and its stability region (in the density-aspect ratio phase diagram) is bounded below by the I phase and above by other LC nonuniform phases such as the smectic (S) or completely ordered crystal (K) phases. At low aspect ratios the I phase can exhibit a direct transition to a plastic crystal (PK) or to a more complex crystalline phase in which particle shapes, orientations, and lattice structures are coupled in a complex fashion. The phase behavior of HDR was studied in detail by Monte Carlo (MC) simulations [1,2] and theory [2–4]. This particle shape, as well as the elliptical one [5–7], can stabilize the I, N, PK, and K phases with HDR exhibiting a region of S stability at high densities. However, a fluid of HR with sufficiently small aspect ratio can also stabilize a tetratic (T) phase [3,7–13] with fourfold symmetry: the orientation distribution function is invariant under $\pi/2$ rotations. This peculiar liquid-crystal texture was also found in experiments on colloidal [14] and nonequilibrium granular [15–18] systems. Particles with a more complex shape, such as zigzag particles or hockey stick–shaped particles, exhibit interesting phase behaviors, such as the increase of S stability with respect to the N phase, by changing the particle shape. The former, having quasi-ideal layers, can be made of particles tilted with respect to the layer normal, and it can also be antiferromorphic [19–21].

The effect of confinement on the phase behavior of two-dimensional or quasi-two-dimensional hard-rod fluids has also been extensively studied [22–26]. The symmetry of the confining external potential can (i) change the relative stability between different LC phases with respect to the bulk and (ii) induce the presence of topological defects in the N director field. On the other hand, mixtures of anisotropic particles in 2D can exhibit, in analogy with their three-dimensional (3D) counterparts, different demixing scenarios [27–29]. However, I-I demixing was not found in mixtures of two-dimensional hard bodies [30].

The aim of the present article is to develop the scaled-particle theory (SPT), a second-virial-based theory for freely rotating hard-triangle (HT) mixtures, to study the phase behavior of the one-component fluid and of certain binary mixtures. Our effort is focused on elucidating the effect of two-body interactions on the symmetry of orientationally ordered phases. Previous experimental, theoretical, and simulation works on equilateral [31–34] and right-angled [34] HT predicted the

*yuri@math.uc3m.es
†ardiaza@math.uc3m.es
‡enrique.velasco@uam.es

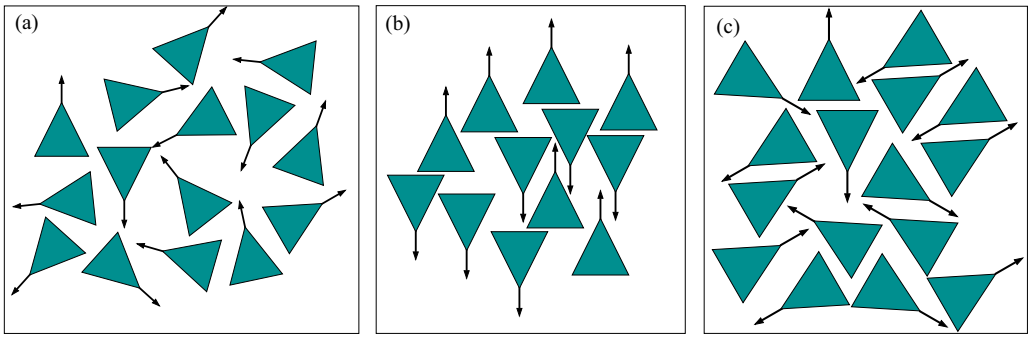

FIG. 1. Sketch of I (a), N (b), and TR (c) uniform phases of HT (the latter two exhibit perfect orientational ordering.

presence of triatic (TR) [31,34] and rhombic (R) [34] nematic phases, respectively, with orientation distribution functions $f(\phi)$ having sixfold [$f(\phi) = f(\phi + \pi/3)$] or eightfold [$f(\phi) = f(\phi + \pi/4)$] symmetries. The controlled synthesis of dispersed colloidal systems, made by microlithography, constitutes an experimental realization of fluids of hard Brownian particles with accurately controlled shapes. The presence of roughness-controlled depletion attractions allows an experimental exploration of dense two-dimensional systems of hard equilateral triangles [31], which constitute systems of hard achiral particles exhibiting local [31] or long-ranged [34] chiral ordering, with the most prominent chirality observed in lattice structures near close packing [34].

This work is focused on the relative stability between the uniform phases of HT: I, N, and TR phases sketched in Fig. 1. In 2D the effect of three- and higher-order correlations becomes crucial to adequately predict the phase behavior of hard particles, especially at high densities. As shown in our previous work [8], the I-T transition densities in a HR fluid dramatically decrease when third-virial contributions are taken into account. We expect the same effect here: inclusion of three-body correlations will certainly enhance the stability of the TR phase with respect to nonuniform phases (the latter are not included in the present study), as predicted by simulations [34]. Also, higher-order correlations can even change the symmetry of the stable phases of HT for specific geometries. For example, right-angled triangles exhibit a stable R phase [34], while SPT predicts N phase stability instead. Despite these differences, we believe a second-virial-based theory is still valuable to systematically study the role of two-body interactions in promoting entropically driven phase transitions in the HT fluid. These interactions predict a N-N first-order phase transition even for the one-component fluid. Also, the I-N transition is of first order for some aspect ratios. Interestingly, simulations on right-angled isosceles triangles also predict a first-order I-R phase transition [34].

The region of stability of the TR phase predicted by SPT extends away from an aspect ratio $\kappa = \sqrt{3}$, and also includes isosceles triangles with wider or more acute opening angles. The second-order I-N transition in the hard needle limit $\kappa \to \infty$ (for acute triangles) or $\kappa \to 0$ (for obtuse triangles) result in different asymptotic expressions for the packing fractions as a function of κ. While in both limits the packing fraction η goes to zero as κ^{-1} (for acute HT) or κ (for obtuse HT), the coefficients of proportionality are different. We also study the phase behavior of symmetric binary mixtures, with species having the same areas and with aspect ratios symmetric with respect to the equilateral triangle: $\kappa_1\kappa_2 = 3$. We found that the mixing of certain symmetric triangles can stabilize the TR phase, which is not stable in the two one-component limits. The phase diagram (in the pressure-composition plane) exhibits second- and first-order I-N transitions, a first-order N-N transition ending in the critical point and, at high pressures, a Landau point where two first-order N-TR transitions and a N-N demixing transition coalesce, resembling the phase-diagram topology of symmetric rod-plate mixtures in 3D [35,36].

The article is organized as follows. Section II is devoted to present the SPT for general mixtures of HT. Analytical expressions for the I-N or I-TR second-order transition lines resulting from a bifurcation analysis are presented, along with some details on the numerical minimization of the free energy with respect to the coefficients of the Fourier expansion of $f_i(\phi)$. In Sec. III expressions for the excluded area of HT mixtures and for the Fourier coefficients, the key ingredients of the theoretical model, are presented. Section IV is devoted to the study of the one-component case. We begin the section by showing the symmetries of the excluded area, which allow us to explain some of the orientational ordering properties of HT. The complete phase diagram of HT (including only uniform phases) is analyzed in detail. In Sec. V phase diagrams are presented for symmetric and asymmetric binary mixtures, the latter exhibiting a strong I-N demixing transition. Finally, some conclusions are drawn in Sec. VI.

II. SPT MODEL FOR A BINARY MIXTURE OF CONVEX BODIES

This section is devoted to presenting expressions for the free energy of a binary mixture of HT using the SPT formalism. The one-component case is trivially obtained by fixing the molar fraction of the corresponding species equal to unity. The binary mixture is described in terms of the one-body density distribution function of species i ($i = 1,2$), $\rho_i(\phi)$, which can be written as

$$\rho_i(\phi) = \rho_i f_i(\phi), \tag{1}$$

with $\rho_i = \rho x_i$ the number density of species i, defined as the product of the total number density ρ (with $\rho = \sum_i \rho_i$) and its molar fraction x_i (which fulfills the constraint $\sum_i x_i = 1$). The function $f_i(\phi)$ is the orientational distribution function of species i, which satisfies $\int_0^{2\pi} d\phi f_i(\phi) = 1$. The total packing

fraction of the mixture is calculated as

$$\eta = \sum_i \rho_i a_i, \tag{2}$$

with a_i the particle area of the corresponding species. According to SPT, the excess part of the free-energy density of a binary mixture of convex 2D bodies reads [8,27,28]

$$\Phi_{\rm ex}[\{\rho_i\}] \equiv \frac{\beta \mathcal{F}_{\rm ex}[\{\rho_i\}]}{A} = -\rho \log(1-\eta) + \frac{\rho^2 \mathcal{K}[\{\rho_i\}]}{1-\eta}, \tag{3}$$

with $\beta = (k_B T)^{-1}$ the inverse temperature, A the total area of the system, and $\mathcal{F}_{\rm ex}[\{\rho_i\}]$ the excess part of the free-energy density functional. We have defined

$$\mathcal{K}[\{\rho_i\}] \equiv \frac{1}{2}\sum_{i,j} x_i x_j \int d\phi_1 \int d\phi_2 f_i(\phi_1) f_j(\phi_2) A_{ij}^{\rm (spt)}(\phi_{12}), \tag{4}$$

where $A_{i,j}^{\rm (spt)}(\phi)$ is related to the excluded area, $A_{ij}^{\rm (excl)}(\phi)$, between species i and j, with a relative angle between their axes equal to ϕ. The corresponding relation is

$$A_{ij}^{\rm (spt)}(\phi) = A_{ij}^{\rm (excl)}(\phi) - a_i - a_j. \tag{5}$$

As usual, the ideal part of the free-energy density is calculated as

$$\Phi_{\rm id}[\{\rho_i\}] \equiv \frac{\beta \mathcal{F}[\{\rho_i\}]}{A} = \sum_i \int d\phi \rho_i(\phi)\big[\log(\rho_i(\phi)\mathcal{V}_i) - 1\big], \tag{6}$$

with $\mathcal{V}_i$ the thermal area of species i. The total free-energy density is simply the sum $\Phi[\{\rho_i\}] = \Phi_{\rm id}[\{\rho_i\}] + \Phi_{\rm ex}[\{\rho_i\}]$. It is useful to express the orientational distribution function $f_i(\phi)$ in terms of its Fourier expansion:

$$f_i(\phi) \equiv \frac{1}{2\pi}\Psi_i(\phi) = \frac{1}{2\pi}\left[1 + \sum_{k\geqslant 1} f_k^{(i)} \cos(k\phi)\right], \tag{7}$$

with $\{f_k^{(i)}\}$ the Fourier amplitudes. Using this expansion the total free-energy per particle in reduced thermal units,

$$\varphi[\{\rho_i\}] \equiv \frac{\Phi[\{\rho_i\}]}{\rho}, \tag{8}$$

can be written as

$$\varphi = \log y - 1 + \sum_i x_i \left\{\log x_i + \frac{1}{2\pi}\int_0^{2\pi} d\phi \Psi_i(\phi)\log\Psi_i(\phi)\right\} + y\mathcal{K}\big(\{f_k^{(i)}\}\big), \tag{9}$$

$$\mathcal{K}\big(\{f_k^{(i)}\}\big) = \frac{1}{2}\sum_{i,j} x_i x_j \sum_{k\geqslant 0} s_k^{(i,j)} f_k^{(i)} f_k^{(j)}, \quad \big(f_0^{(i)} = 1\big), \tag{10}$$

where the constant terms $2\pi\mathcal{V}_i$ have been dropped. Also, we defined $y \equiv \frac{\rho}{1-\eta}$ and the coefficients

$$s_k^{(i,j)} = \frac{1}{2\pi}\int_0^{2\pi} d\phi A_{ij}^{\rm (spt)}(\phi)\cos(k\phi). \tag{11}$$

According to SPT [27], the pressure is calculated from

$$\beta p = \frac{\partial \Phi_{\rm ex}}{\partial \eta} = y + y^2 \mathcal{K}\big(\{f_k^{(i)}\}\big), \tag{12}$$

and the Gibbs free-energy per particle in reduced thermal units, for a fixed value of the pressure p_0, is

$$g = \varphi + \beta p_0(\langle a\rangle + y^{-1}), \quad \langle a\rangle = \sum_i x_i a_i. \tag{13}$$

From the equality $p = p_0$ we obtain

$$y = \frac{\sqrt{1 + 4\beta p_0 \mathcal{K}\big(\{f_k^{(i)}\}\big)} - 1}{2}. \tag{14}$$

The partial derivatives of the Gibbs free-energy per particle g with respect to the Fourier coefficients $f_k^{(i)}$ are given by

$$\frac{\partial g}{\partial f_k^{(i)}} = x_i \left\{\frac{1}{2\pi}\int_0^{2\pi} d\phi \cos(k\phi)\log\Psi_i(\phi) + y\sum_j x_j s_k^{(i,j)} f_k^{(j)}\right\}, \quad k \geqslant 1. \tag{15}$$

Defining $x \equiv x_1$ (so that $x_2 = 1 - x$), we fix p_0 and, from (14), obtain $y(x)$. Substitution in (13) provides the Gibbs free energy $g(x)$ as a function of the mixture composition. The values of the Fourier coefficients $\{f_k^{(i)}\}$ are those which minimize the Gibbs free energy g. A conjugate-gradient minimization was implemented, with analytical gradients calculated from (15) and with a number of Fourier components ranging from 20 to 50 for each species. Their precise values depend on the sharpness of the functions $f_i(\phi)$. The common-tangent construction on $g(x)$ gives the coexistence conditions.

Alternatively, coexistence can be calculated through the equality of the chemical potential of species i belonging to different coexisting phases. These are calculated from

$$\beta\mu_i = \log(y x_i) + \frac{1}{2\pi}\int_0^{2\pi} d\phi \Psi_i(\phi)\log\Psi_i(\phi) + y\sum_j x_j \sum_k s_k^{(i,j)} f_k^{(i)} f_k^{(j)} + \beta p_0 a_i, \tag{16}$$

where p_0 is a fixed value of pressure, and y is calculated from (14), while $\{f_k^{(i)}\}$ are calculated from Gibbs free-energy minimization. The degree of orientational order of species i is measured by the N ($k = 2$) and TR ($k = 6$) order parameters:

$$Q_k^{(i)} = \int_0^{2\pi} d\phi f_i(\phi)\cos(k\phi), \quad k = 2, 6. \tag{17}$$

The packing fraction of the second-order I-(N,TR) transition can be calculated by expanding the expression $\frac{\partial g}{\partial f_k^{(i)}}$ given by Eq. (15) up to first order in $f_k^{(i)}$ ($k = 2$ for the N and $k = 6$ for the TR phase). The equilibrium condition is obtained by equating the result to zero, which can be written in matrix

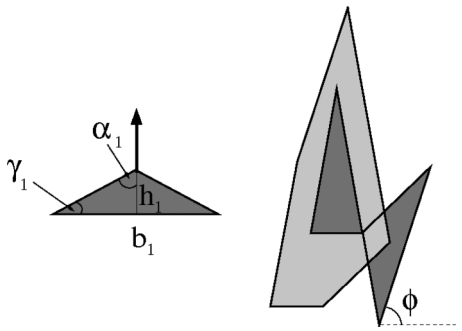

FIG. 2. Sketch of the excluded area between two HT with relative angle between their axes equal to ϕ. The main parameters (base, height, angles) used to define the geometry of the triangle are labeled.

form as

$$R\boldsymbol{f}_k = \boldsymbol{0}. \tag{18}$$

Here we defined the vector $\boldsymbol{f}_k \equiv (f_k^{(1)}, f_k^{(2)})^{\mathrm{T}}$, while the R-matrix elements are

$$R_{ij} \equiv \delta_{ij} + 2yx_j s_k^{(i,j)}, \tag{19}$$

with δ_{ij} the Kronecker delta. The linear system (18) has a nontrivial solution if $\det(R) = 0$, which implies that the packing fraction at the transition is

$$\eta^* = \frac{2 + \Delta_0 - \sqrt{\Delta_0^2 - 4\Delta_1}}{2(1 + \Delta_0 + \Delta_1)}, \tag{20}$$

where we have defined

$$\Delta_0 = -\frac{2}{\langle a\rangle}\left(x_1 s_k^{(1,1)} + x_2 s_k^{(2,2)}\right), \tag{21}$$

$$\Delta_1 = \frac{4x_1x_2}{\langle a\rangle^2}\left[s_k^{(1,1)} s_k^{(2,2)} - \left(s_k^{(1,2)}\right)^2\right]. \tag{22}$$

III. EXCLUDED AREA BETWEEN TWO HT

The excluded area between two isosceles triangles of base b_i and heights h_i ($i = 1,2$) with main axes at a relative angle ϕ is sketched in Fig. 2. The main axis is defined in the direction of the particle height, i.e., pointing from the base to the opposite vertex. The aspect ratio of species i is $\kappa_i = 2h_i/b_i$, and $\alpha_i = \arctan(\kappa_i^{-1})$ is the angle between the height and the equally sized lengths. $\gamma_i = \pi/2 - \alpha_i = \arctan(\kappa_i)$ is the angle between the latter and the base. We also define the angles $\alpha_{ij} = \alpha_i + \alpha_j$ and $\theta_{ij} = \arctan[\frac{1}{2}(\kappa_i + \kappa_j)]$. For the case where the aspect ratios fulfill the relation $\kappa_i\kappa_j \geqslant 3$, the functions $A_{ij}^{(\mathrm{spt})}(\phi)$ can be calculated as

$$A_{ij}^{(\mathrm{spt})}(\phi) = \begin{cases} (b_ih_j + b_jh_i)\cos\phi, & 0 \leqslant \phi \leqslant \alpha_{ij}, \\ \frac{1}{2}(b_ih_j + b_jh_i)\cos\phi + \left(h_ih_j - \frac{1}{4}b_ib_j\right)\sin\phi, & \alpha_{ij} \leqslant \phi \leqslant \theta_{ij}, \\ -\frac{1}{2}(b_ih_j + b_jh_i)\cos\phi + \left(h_ih_j - \frac{3}{4}b_ib_j\right)\sin\phi, & \theta_{ij} \leqslant \phi \leqslant \pi. \end{cases} \tag{23}$$

For $\kappa_i\kappa_j \leqslant 3$ we obtain

$$A_{ij}^{(\mathrm{spt})}(\phi) = \begin{cases} (b_ih_j + b_jh_i)\cos\phi, & 0 \leqslant \phi \leqslant \theta_{ij}, \\ b_ib_j\sin\phi, & \theta_{ij} \leqslant \phi \leqslant \alpha_{ij}, \\ -\frac{1}{2}(b_ih_j + b_jh_i)\cos\phi + \left(h_ih_j - \frac{3}{4}b_ib_j\right)\sin\phi, & \alpha_{ij} \leqslant \phi \leqslant \pi. \end{cases} \tag{24}$$

For angles $\pi < \phi \leqslant 2\pi$ this function can be calculated by invoking its symmetry with respect to π: $A_{ij}^{(\mathrm{spt})}(\pi + \phi) = A_{ij}^{(\mathrm{spt})}(\pi - \phi)$ (with $\phi \in [0,\pi]$).

Defining the angles $\gamma_{ij}^{\pm} = \gamma_i \pm \gamma_j$, the coefficients $s_k^{(i,j)}$ in (11) can be calculated as

$$s_1^{(i,j)} = \frac{c_{ij}}{2}\left(\theta_{ij} - \frac{\gamma_{ij}^+}{2}\right)\sin\gamma_{ij}^+, \tag{25}$$

$$s_k^{(i,j)} = -\frac{c_{ij}(1+\delta_{k0})}{2(k^2-1)}\{(-1)^k[\cos(k\gamma_{ij}^+) + 2\cos\gamma_{ij}^- + \cos\gamma_{ij}^+] + 2\sqrt{1 + 2\cos\gamma_{ij}^-\cos\gamma_{ij}^+ + \cos^2\gamma_{ij}^-}\cos(k\theta_{ij})\},$$
$$k \neq 1, \tag{26}$$

where

$$c_{ij} = \frac{l_il_j}{\pi} = \frac{1}{\pi}\sqrt{a_ia_j} \times \sqrt{\left(\kappa_i + \frac{1}{\kappa_i}\right)\left(\kappa_j + \frac{1}{\kappa_j}\right)}, \tag{27}$$

with $l_i = \sqrt{h_i^2 + (b_i/2)^2}$ the equally sized lengths of triangle i, and $a_i = b_ih_i/2$ its particle area.

IV. ONE-COMPONENT FLUID

Figure 3 shows the function $A^{(\mathrm{spt})}(\phi) \equiv A_{11}^{(\mathrm{spt})}(\phi)$, scaled by $2a$ ($a = a_1$), for four different values of aspect ratio corresponding to triangles with $\kappa \geqslant \sqrt{3}$ (a) and $\kappa_1 \leqslant \sqrt{3}$ (b). For the sake of brevity, in this section we drop the species labels in all the magnitudes defined in the preceding section.

As can be seen from the figure, this function has a rather complex form: it may have up to three local minima and three local maxima in the interval $[0,\pi]$. The absolute minimum is reached at $\phi = \pi$, for which the excluded volume is $A^{(\mathrm{excl})} = 4a$, while for $\phi = 0$ the function $A^{(\mathrm{spt})}(\phi)$ has a local maximum corresponding to $A^{(\mathrm{excl})} = 6a$. The absolute maximum is always located in the interval $[\pi/2,\pi)$ and its position tends to $\pi/2$ as the aspect ratio moves away from $\sqrt{3}$ (the value corresponding to the equilateral triangle) in both directions: $\kappa \to \infty$ or $\kappa \to 0$. It is interesting to note that for

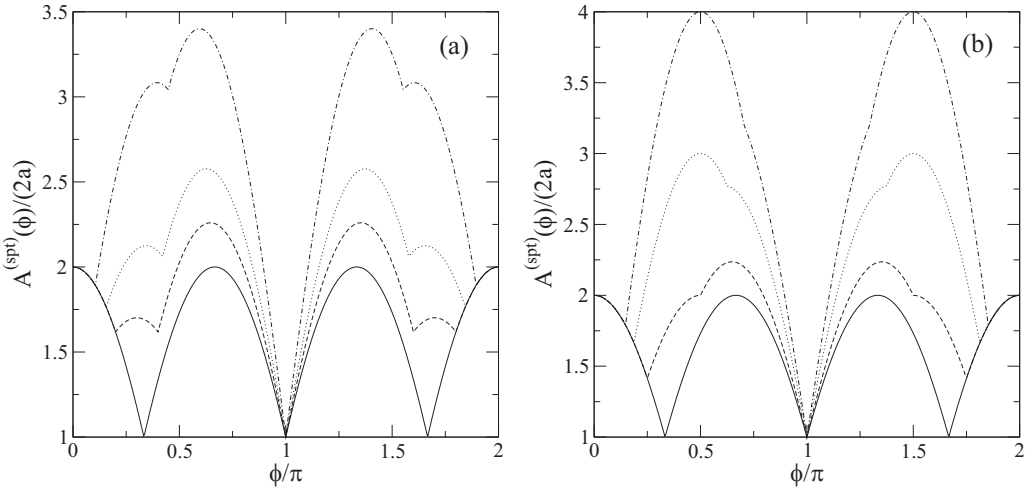

FIG. 3. (a) The function $A^{(\mathrm{spt})}(\phi)/(2a)$ for triangles with $\kappa \geqslant \sqrt{3}$. Chosen values are $\kappa = \sqrt{3}$ (solid), $\sqrt{5+2\sqrt{5}}$ (dashed), 4 (dotted), and 6 (dot-dashed). (b) The same function for triangles with $\kappa \leqslant \sqrt{3}$ and values: $\sqrt{3}$ (solid), 1 (dashed), 2/3 (dotted), and 1/2 (dot-dashed).

$\kappa = \sqrt{5+2\sqrt{5}}$, the aspect ratio corresponding to the sublime triangle (that for which the ratio between the equally sized lengths and the base of the triangle is just the golden ratio), two of the local minima of $A^{(\mathrm{spt})}(\phi)$ have exactly the same value. As we will see later, the presence of local minima in the excluded area imposes some important symmetries in the orientational distribution function $f(\phi)$. For equilateral triangles ($\kappa = \sqrt{3}$) the excluded area has a sixfold symmetry: the local maxima and local minima have the same heights, and the former are located at $n\pi/3$ with $n = 0,1,\ldots,6$. This symmetry forces the orientational distribution function of the nematic phase to have a periodicity of $\pi/3$: $h(\phi) = h(\phi + \pi/3)$. This phase, called the TR phase, has six equivalent nematic directors.

For the one-component case (dropping the species indexes), the expressions for the coefficients (11) are more conveniently written as

$$s_k = \begin{cases} \frac{8l^2}{\pi}\cos^4\left(\frac{\gamma}{2}\right), & k = 0, \\ 0, & k = 1, \\ -\frac{4l^2}{\pi(4j^2-1)}\left\{\cos\left[\frac{(2j-1)\gamma}{2}\right]\cos\left[\frac{(2j+1)\gamma}{2}\right]\right\}^2, & k = 2j,\ j \geqslant 1, \\ \frac{l^2}{\pi j(j+1)}\{\sin(j\gamma)\sin[(j+1)\gamma]\}^2, & k = 2j+1,\ j \geqslant 1. \end{cases} \tag{28}$$

The fact that the even coefficients s_{2j} (for $j \geqslant 1$) are always negative while the odd ones are positive has an important implication on the orientational properties of HT, namely, the absence of a polar N phase, as we prove in the Appendix.

For the one-component fluid the packing fraction corresponding to the second-order I-(N,TR) transition can be obtained from (20)–(22) by taking $x_1 = 1$. The result is

$$\eta_n^* = (1+\Delta_0)^{-1} = \left[1 + \frac{2}{(n^2-1)\pi}(\kappa + \kappa^{-1})(\cos(n\gamma) + \cos\gamma)^2\right]^{-1}, \quad n = 2,6. \tag{29}$$

For the particular case $n = 2$ (corresponding to the I-N bifurcation), using $\tan\gamma = \kappa$, this can be rewritten as

$$\eta_2^* = \left[1 + \frac{2}{3\pi}(\kappa + \kappa^{-1})\left(1 - \frac{2}{\sqrt{\kappa^2+1}}\right)^2\left(1 + \frac{1}{\sqrt{\kappa^2+1}}\right)^2\right]^{-1}. \tag{30}$$

It is easy to see that this expression is not symmetric with respect to the change $\kappa \to \kappa^{-1}$. The limits $\kappa \to \infty$ and $\kappa \to 0$ (both corresponding to the same hard-needle limit) are not equivalent. Asymptotically we obtain $\eta_2^* \approx \frac{3\pi}{2\kappa}$ for the former and $\eta_2^* \approx \frac{3\pi\kappa}{8}$ for the latter. The TR phase is expected to be stable in some interval of aspect ratios $[\kappa_1^*,\kappa_2^*]$, including the value for the equilateral triangle ($\kappa = \sqrt{3}$), for which TR is the only possible orientationally ordered uniform phase. An estimation of this interval is obtained by solving the equality $\eta_2^*(\kappa) = \eta_6^*(\kappa)$ for κ. At these points, the I-N and I-TR second-order transition curves intersect, the latter being below the former for aspect ratios values in the interval $[\kappa_1^*,\kappa_2^*]$. From (29), this equation is equivalent to finding the values of γ ($\kappa = \tan\gamma$) for which

$$r\cos(2\gamma) + (r-1)\cos(\gamma) = \cos(6\gamma), \tag{31}$$

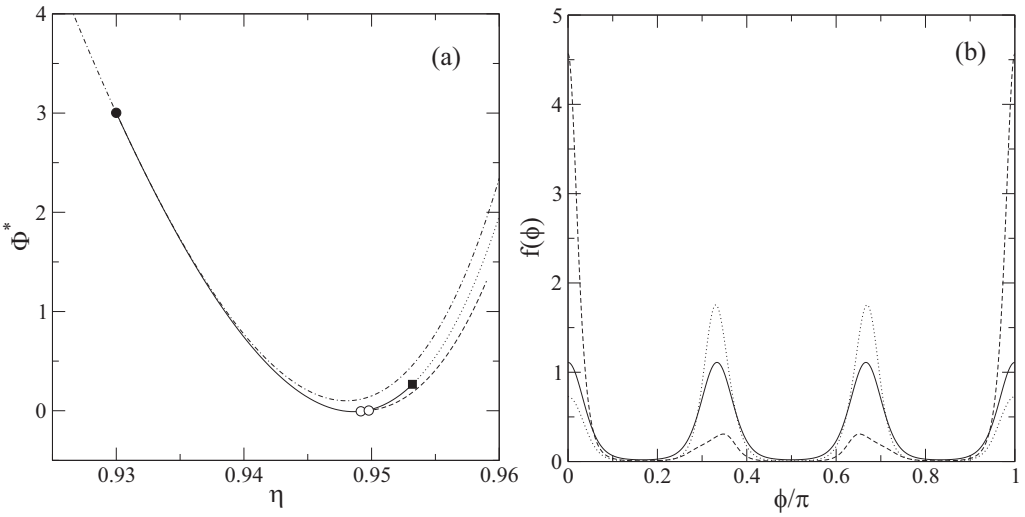

FIG. 4. (a) Free-energy densities minus a straight line: $\Phi^* \equiv \Phi - a\eta - b$ (with $a = 623.45$ and $b = -562.94$) corresponding to the I (dot-dashed), TR (solid), N (dashed), and TR* (dotted) phases of HT with $\kappa = 2.2$. The solid circle indicates the I-TR bifurcation, while open circles represent the TR-N coexistence (with $\eta_{\rm TR} = 0.949\,157$ and $\eta_{\rm N} = 0.949\,785$) and the square shows the N-TR* bifurcation. (b) Orientation distribution functions corresponding to TR (solid) at $\eta = 0.949$, N (dashed) at $\eta = 0.95$, both for stable phases of HT with $\kappa = 2.2$. Dotted line is a distribution function corresponding to a TR* metastable phase with $\eta = 0.957$.

with $r = \pm\sqrt{\frac{35}{3}}$. This gives the values $\kappa_1^* = 1.278$ and $\kappa_2^* = 2.405$. However, this result is correct only if the involved phase transitions are of second order, which is not the case, as we will promptly see.

As already pointed out, the TR phase is also stable for aspect ratios in the neighborhood of $\sqrt{3}$, corresponding to the equilateral triangle aspect ratio. The sequence of stable phases for $\kappa = 2.2 > \sqrt{3} \approx 1.73$ as η is increased is shown in Fig. 4(a), where the free-energy densities of different stable and metastable branches are plotted. The I phase is stable up to $\eta \approx 0.93$, at which the TR phase bifurcates through a second-order I-TR transition. The latter is stable up to $\eta_{\rm TR} = 0.949\,157$, the coexisting value of the first-order TR-N transition. The orientational distribution function of the TR phase for $\eta = 0.949$ (just below the TR-N transition) is shown in Fig. 4(b); it has the expected symmetry $f(\phi + \pi/3) = f(\phi)$. Also, we show the orientational distribution function of the N phase for $\eta = 0.95$ (above the transition). We notice the strong uniaxial ordering of HT at $\phi = \{0,\pi\}$, although the presence of small peaks at $\phi \approx \{\pi/3, 2\pi/3\}$ can be also seen. From $\eta_{\rm N} = 0.949\,785$ onward the N phase is the stable phase up to close packing. It is interesting to see that the metastable TR phase changes continuously at $\eta = 0.9532$ to a different asymmetric TR* phase [see panel (b)], with two sharp, equivalent peaks at $\phi \approx \{\pi/3, 2\pi/3\}$, while the other two peaks at $\phi = \{0,\pi\}$ have considerably lower heights. This TR* phase is always metastable with respect to the usual uniaxial N phase. The

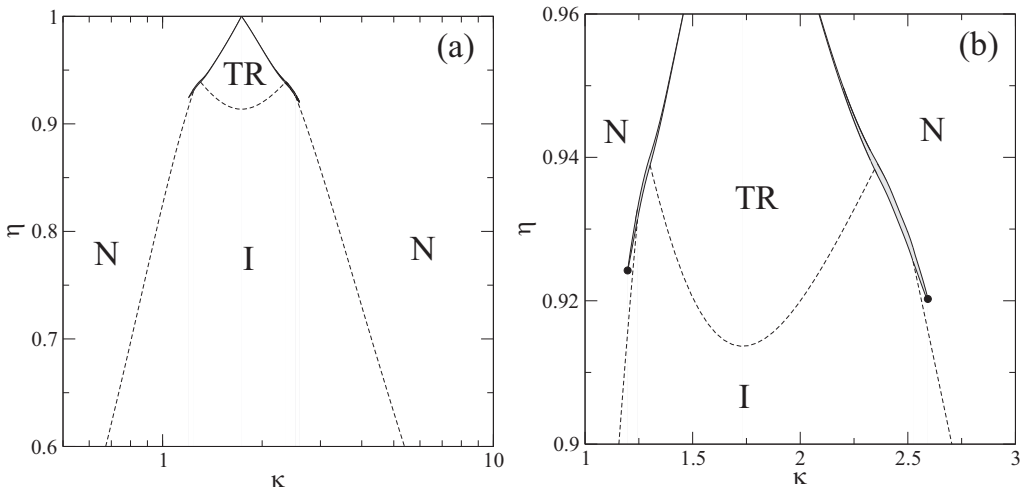

FIG. 5. Phase diagram of HT in the packing-fraction (η)-aspect ratio (κ) plane. (a) $\eta \in [0.6, 1]$ in logarithmic scale for κ. (b) Zoom of the phase diagram (with κ in linear scale), showing the presence of N-N transitions ending in critical points (solid circles), the first-order character of the I-N transition for certain values of κ, and the region of stability of the TR phase. Dashed and solid lines show second- and first-order transitions, respectively. Regions of stability of different phases are correspondingly labeled.

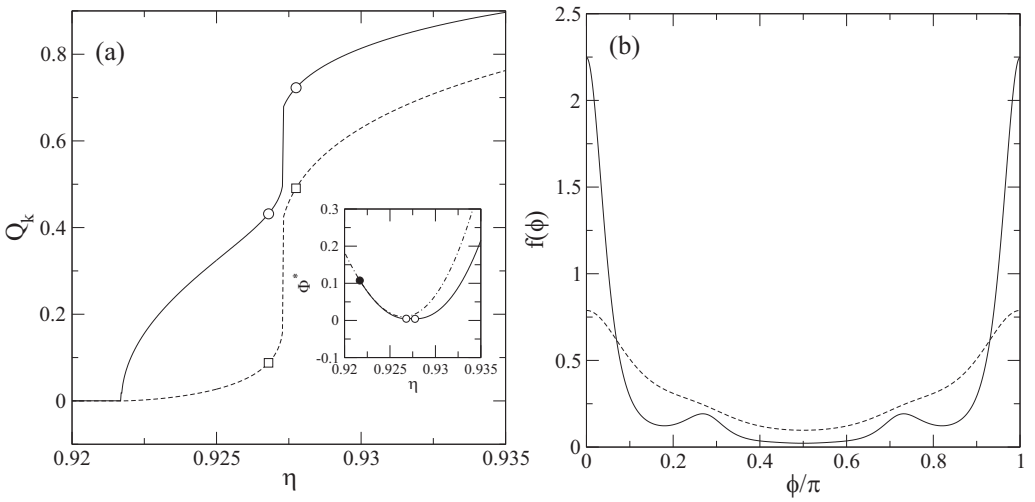

FIG. 6. (a) Order parameters Q_k (solid for $k = 2$ and dashed for $k = 6$) as a function of the packing fraction η for HT with $\kappa = 1.215$, showing the N_1-N_2 first-order transition (shown with circles and squares, respectively). Inset: free-energy densities minus a straight line, $\Phi^* = \Phi - a\eta - b$ (with $a = -288.33$ and $b = 334.6$), corresponding to the I (dot-dashed) and N_i (solid) phases as a function of η. The solid circles indicates the I-N bifurcation point, while the open circles show the N-N coexistence values. (b) Orientation distribution functions corresponding to the coexisting N_1 (dashed) and N_2 (solid) phases for the packing-fraction values $\eta_1 = 0.926\,80$ and $\eta_2 = 0.927\,76$, respectively.

same sequence of stable and metastable phases is found for $\kappa \lesssim \sqrt{3}$. We note here that MC simulations of equilateral HT found the I-TR transition at $\eta \approx 0.7$, with the TR phase being stable up to $\eta \approx 0.89$, where a transition to a chiral triangular crystal takes place [34]. In this sense the I-(TR,N) transition packing fractions estimated by the SPT for $\kappa \approx \sqrt{3}$ are clearly overestimated. We expect that the inclusion of three-body correlations in a modified theory will correct the transition densities, as we have already demonstrated for the HR fluid [8].

The complete phase diagram of HT is shown in Fig. 5. The second-order transitions are shown with dashed lines, while the binodals of the first-order transitions are shown with solid lines. The first-order transitions are so weak that the coexistence regions are not visible in the scale of the graph. As pointed out before, the asymmetric character of the second-order I-N transitions, as $\kappa \to \infty$ and $\kappa \to 0$, is apparent. The TR phase is stable in an interval of aspect ratios about $\sqrt{3}$, but the interval is now modified with respect to the values obtained from the bifurcation analysis due to the first-order character of the I-N and TR-N transitions for some values of κ. Now the extrema of this interval are $\kappa_1^* = 1.30$ and $\kappa_2^* = 2.35$, the values corresponding to the critical end points where the second-order I-TR transition line meets the I (from below) and TR (from above) binodals of the I-N and TR-N first-order transitions, respectively. The TR phase is bounded from above by the TR-N first-order transition, although we cannot discard the presence of tricritical points for values of κ close to $\sqrt{3}$, where the TR-N transition would become of second order. The numerical procedure used to calculate the TR-N coexistence becomes unstable for values of η close to 1, so we have extrapolated the binodals up to close packing, $\eta = 1$.

But the most striking feature of the phase diagram is the presence of first-order N-N transitions at both sides of $\sqrt{3}$, both ending in critical points $\kappa_1^c \approx 1.2$ and $\kappa_2^c \approx 2.6$ [see panel (b)]. When changing these values of aspect ratios to $\kappa = \sqrt{3}$, these N-N transitions meet the second-order I-N transition at two critical end points, and from these points we find the first-order I-N transitions already described. To the best of our knowledge this is the first example where a N-N transition is found for a one-component hard-particle system.

Figure 6(a) shows the order parameters Q_k ($k = 2,6$) as a function of η for $\kappa = 1.215$, a value for which a N-N transition takes place. We can see the abrupt changes in order parameters as η is increased. The coexistence values of η are indicated on the curves as symbols, while the inset shows the free-energy densities of the I and N phases, together with the coexistence points found from the usual double-tangent construction. The orientational distribution functions corresponding to the coexisting N phases are plotted in panel (b). We notice the difference in orientational ordering: while the less dense N is sightly ordered, particles in the other phase are strongly oriented along the uniaxial director. The presence of small peaks at $\phi \approx \{\pi/3, 2\pi/3\}$ is due to the rather small orientational TR correlations, as the aspect ratio is not too far from $\sqrt{3}$.

V. BINARY MIXTURES

Now we present results obtained from the numerical implementation of SPT as applied to a particular symmetric mixture of HT. In this mixture, the aspect ratios of the two species fulfill the condition $\kappa_1\kappa_2 = 3$ and have equal areas, $a_1 = a_2$. The ratio between their bases is chosen to be $r = b_2/b_1 = 1.453$. Obviously the results will not depend on the particular value of one of the bases, so we set $b_1 = 1$. We obtain $\kappa_1 = \sqrt{3}r = 2.52$ and $\kappa_2 = \sqrt{3}/r = 1.19$. Note that these values are outside the interval [1.3,2.35] inside which the TR phase is stable in the one-component system. The chosen particle symmetry gives $\alpha_{ij} = \theta_{ij}$, so the interval $[\alpha_{ij}, \theta_{ij}]$ in the expressions for $A_{ij}^{(\mathrm{spt})}(\phi)$, given by Eqs. (23) and (24), shrinks to zero and both expressions become equivalent. The consequence of this

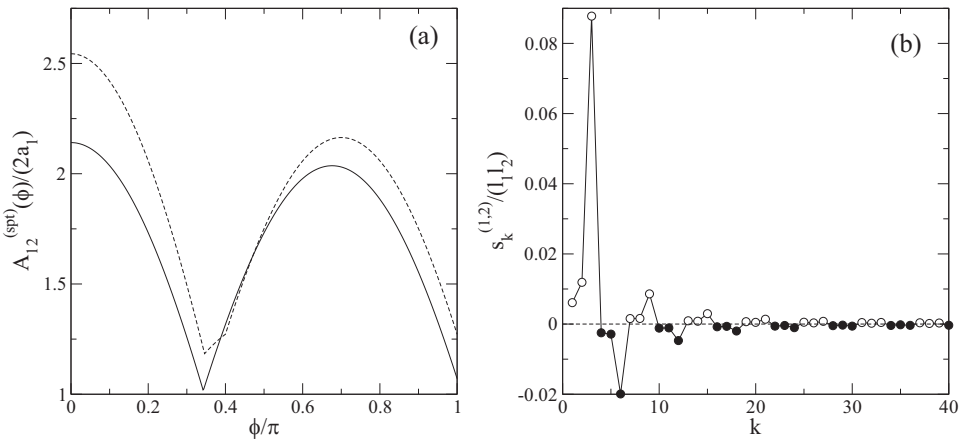

FIG. 7. (a) The function $A_{12}^{(\mathrm{spt})}(\phi)$ related to the excluded areas between two symmetric ($\kappa_1\kappa_2 = 3$) triangles of equal areas ($a_1 = a_2$) and $r = b_2/b_1 = 1.453$ (solid), and between the sublime and Gnomon (with a ratio between its base and the equally sized lengths equal to the golden number) triangles of equal areas (dashed). (b) Scaled Fourier coefficients of the pair of species corresponding to the solid line in (a). Open and solid circles correspond to positive and negative coefficients, respectively.

symmetry can be seen in Fig. 7(a), where we plot the functions $A_{12}^{(\mathrm{spt})}(\phi)$ for the previously defined pair of symmetric triangles and also for a nonsymmetric pair. Note how the vanishing of the interval $[\alpha_{ij},\theta_{ij}]$ makes the excluded area much more similar to that of equilateral triangles. As we will promptly see, this property has a profound impact on the relative stability of the TR phase in binary mixtures. The previously reported property of the one-component fluid, namely, the positiveness (negativeness) of odd (even) Fourier coefficients, does not have a counterpart in binary mixtures, as can be seen from Fig. 7(b). Therefore, the previous proof on the absence of a polar phase in the one-component fluid of HT looses its validity for binary mixtures. Because of this point, we were forced to use all the Fourier coefficients in the free-energy minimization. However, for all the pairs of triangles explored, we always obtained free-energy minima with vanishing odd Fourier coefficients so that the polar phase can probably be discarded.

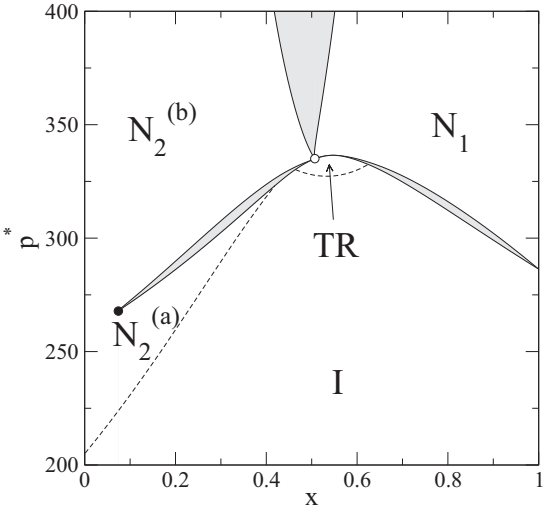

FIG. 8. Phase diagram in the scaled pressure ($p^* = \beta p a_1$)-molar fraction ($x \equiv x_1$) plane of the HT with $\kappa_1 = 2.52$ (species 1) and its symmetric ($\kappa_1\kappa_2 = 3$) counterpart, both of equal areas and with $r = b_2/b_1 = 1.453$. Regions of stability of different phases are correspondingly labeled. Dashed and solid lines represent the second-order transition curves and the binodals of first-order transitions, respectively. Coexistence regions are shaded in gray. The solid and open circles represent the critical and Landau points, respectively.

The phase diagram of the symmetric binary mixture ($\kappa_1\kappa_2 = 3$) with equal particle areas and $r = b_2/b_1 = 1.453$ is shown in Fig. 8 in the reduced pressure-composition plane. Species 1, having aspect ratio $\kappa_1 = 2.52 > \sqrt{3}$, corresponds to an acute-angled triangle with $\gamma_1 > \pi/3$, while the other one, with $\kappa_2 = 1.19 < \sqrt{3}$, is also an acute-angled triangle but with $\gamma_2 < \pi/3$. A second-order I-N_2 transition line departs from the $x \equiv x_1 = 0$ axis, terminating at the critical end point where it meets from below (above) the $N_2^{(a)}$ (I) binodal of the $N_2^{(a)}$-$N_2^{(b)}$ (I-$N_2^{(b)}$) transition. As pointed out before, the one-component fluid of HT with $\kappa < \sqrt{3}$ exhibits a N-N transition for $\kappa \in [1.2,1.24]$. The aspect ratio $\kappa_2 = 1.19$ of species 2 is below this interval, so this transition cannot end with $x = 0$ but instead it ends in a critical point. Also the one-component HT fluid with $\kappa > \sqrt{3}$ exhibits a N-N transition for $\kappa \in [2.52,2.60]$ and a I-N first-order transition for $\kappa \in [2.34,2.52]$, which turns into a TR-N transition for $\kappa < 2.34$ [see Fig. 5(b)]. The aspect ratio $\kappa_1 = 2.52$ coincides with one of the limits of both intervals, so the first-order I-N_1 transition in the binary mixture this time ends at $x = 1$. We found that the present mixture exhibits a second-order I-TR transition ending at the I binodal of the I-$N_2^{(b)}$ transition (on the left) and at the I binodal of the I-N_1 transition (on the right). Above this line there exists a region of TR phase stability, bounded above by the TR binodal of the first-order TR-N_i transitions. Both transitions coalesce at a Landau point above which there appears a N_1-$N_2^{(b)}$ demixing transition with a demixed gap that increases with pressure. It is interesting to note the similarity between this phase diagram and that of a symmetric binary mixture of rods and plates in three dimensions (with species of equal volumes and aspect ratios satisfying $\kappa_1\kappa_2 = 1$): the first-order I-N transitions departing from $x = 0$ and $x = 1$ end at the Landau point, above which there is either N-N demixing or a small region of biaxial nematic phase stability bounded above

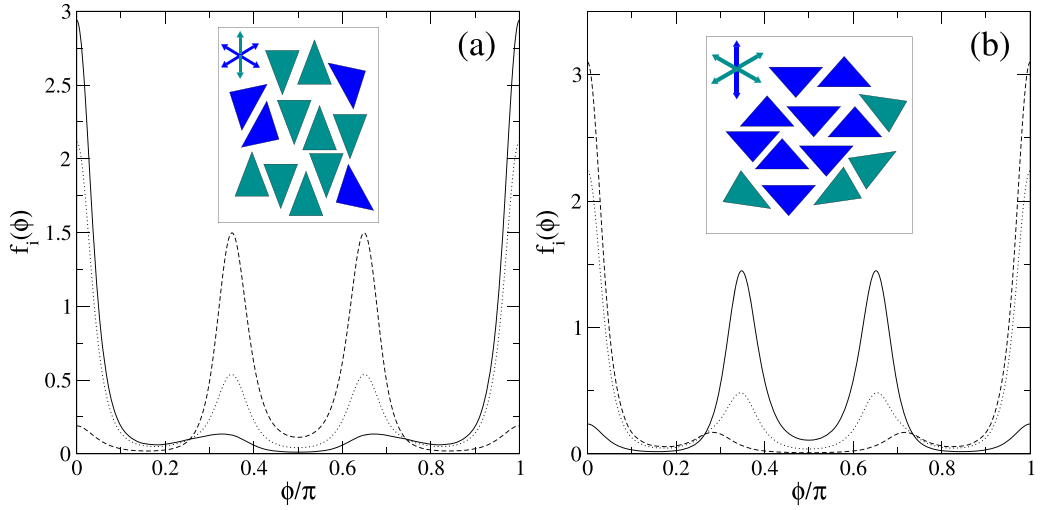

FIG. 9. Distribution functions of the first (solid) and second (dashed) species of the same binary mixture as in Fig. 8 for a fixed scaled pressure $p^* = 346.042$ and molar fractions $x = 0.7$ (a) and $x = 0.3$ (b). Dotted lines indicate the total orientation distribution function $f_t(\phi)$ (see text for definition). Insets are schematic particle configurations for binary mixtures corresponding to each of the subfigures (for simplicity, perfect orientational ordering was assumed with arrows indicating the orientations of particle axes).

by N-N demixing. The most important conclusion that can be drawn from the topology of the phase diagram shown in Fig. 8 is that by appropriately choosing the triangular geometries of the species (i.e., their symmetrization), the TR phase can be stabilized in mixtures of species which by themselves cannot stabilize this phase in their corresponding one-component phase diagrams.

The orientational ordering of different species at pressures above the Landau point in the regions of N phase stability is shown in Fig. 9. At $x = 0.7$ species 1, with a higher composition, possesses an orientational distribution function with a clear uniaxial nematic symmetry: two sharp peaks located at 0 and π, with rather small TR correlations at $\pi/3$ and $2\pi/3$. But the axes of the second species exhibit two clear sharp peaks at $\sim\pi/3$ and $\sim 2\pi/3$, while their proportion for orientations along 0 and π is very small. This orientational segregation of species implies that the total orientational distribution function, defined as $f_t(\phi) = \sum_i x_i f_i(\phi)$, has two main peaks located at 0 and π, indicating the uniaxial character of the N phase; but strong TR correlations are present, as indicated by the fact that the other two orientations have well-developed peaks. A similar situation occurs at the other side of the phase diagram, for $x = 0.3$. Now the second species has a clear uniaxial N symmetry, while the axes of the first species point to the other two directions, $\{\pi/3, 2\pi/3\}$, to give a total orientational distribution function $f_t(\phi)$ with four clear peaks at $n\pi/3$ ($n = 0,1,2,3$).

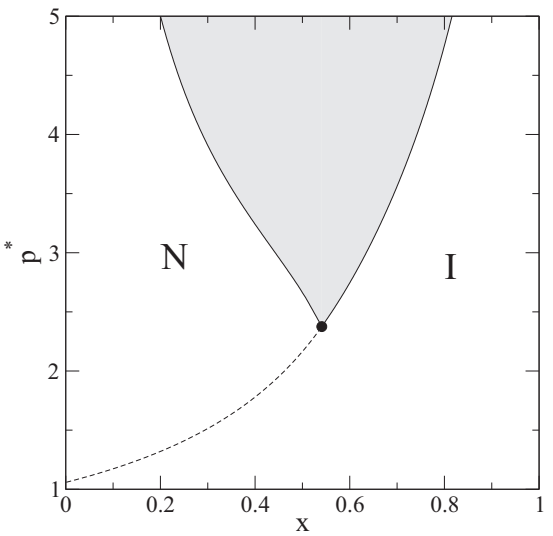

FIG. 10. Phase diagram of a binary mixture of the sublime triangle (species 1) and a triangle with $\kappa_2 = 5\kappa_1$, both having the same area.

To end this section we show in Fig. 10 the usual I-N demixing scenario above a tricritical point occurring in binary mixtures of species with equal areas and sufficiently different aspect ratios. The I-N and N-N demixing was also found in mixtures of two-dimensional particles with other shapes (discorectangles, rectangles and ellipses [27–29]), and they are well documented in mixtures of three-dimensional hard anisotropic bodies [37–41]. We have chosen triangles with $\kappa_1 = \sqrt{5 + 2\sqrt{5}}$ (the sublime triangle) and $\kappa_2 = 5\kappa_1$, and with the same particle areas. The second-order I-N transition departs from the one-component fluid $x = 0$ and extends up to a tricritical point above which the mixture exhibits strong demixing. We should note that, at higher pressures, the I-N second order transition departing from the one-component fluid at $x = 1$ should meet the I binodal of the I-N demixing region at a critical end point. The value of the corresponding pressure at this point is so high that our numerical scheme to find I-N coexistence, based on a Fourier expansion, becomes unstable.

VI. CONCLUSIONS

We used SPT to study the phase behavior of the one-component HT fluid, focusing on a study of the relative stability and phase transitions between uniform phases. Isosceles HT exhibit a fascinating and rich phase diagram. We have shown

that the TR phase exists not only for the equilateral triangles (with $\kappa = \sqrt{3}$), but also for a certain range of aspect ratios including this value. Also, we have found the presence of N-N transition ending in critical points for triangles with aspect ratios inside small intervals at both sides of $\sqrt{3}$. This is an example of one-component hard-particle systems exhibiting a N-N phase transition. We found that the I-N transition becomes of first order for aspect ratios less (greater) than the values $\kappa_1^{(\mathrm{cep})} > \sqrt{3}$ ($\kappa_2^{(\mathrm{cep})} < \sqrt{3}$), corresponding to two critical end points where the I-N second-order line meets one of the binodals of the N-N transition at both sides of $\sqrt{3}$. For packing fractions below these values, the I-N transition is of second order, with the transition curve being asymmetric with respect to the change $\kappa \to \kappa^{-1}$: the obtuse triangles stabilize the N phase at lower packing fractions than the acute ones. The second-order I-TR line intersects the I binodals of the first-order I-N transitions at two critical end points that define the limits of the TR phase stability region, which in turn is bounded above by first-order TR-N transitions.

Using the same formalism we have also studied some particular binary mixtures of HT. The main purpose was to elucidate if the mixing of triangles of certain geometries can stabilize a TR phase even when this phase is not stable in the two one-component limits. We have shown that if the species are symmetric with respect to $\sqrt{3}$, namely, (i) their aspect ratios fulfill the condition $\kappa_1\kappa_2 = 3$ and (ii) they have equal particle areas, there exists a range of aspect ratios, beyond that of the one-component fluid, for which a region of a stable TR phase does exist. We computed the phase diagram (in the pressure-composition plane) for one of these particular mixtures which exhibits a fascinating topology, i.e., the presence of first-order I-N and N-N transitions, the latter ending in a critical point. These transitions coalesce, at higher pressures, with the I-TR second-order transition line and further continue as two first-order TR-N transitions meeting at a Landau point. The TR binodals of both TR-N transitions are just the upper bounds of the region of TR stability. Finally, N binodals of a new N-N demixing transition depart from this Landau point, with a demixing gap strongly increasing with pressure. This phase diagram resembles that of a binary symmetric mixture of rods and plates: the presence of a Landau point at the coalescence of both I-N transition curves, and N-N or biaxial N phase stability regions above, depending on the value of aspect ratios [35,36].

To end this section, we remark that the density expansion of the SPT is exact up to the second order, i.e., it recovers the exact second-virial coefficient while it approximates the higher-order ones. In 2D the third- and higher-order virial coefficients, when properly scaled with the second virial coefficient, do not vanish at the Onsager limit. Therefore, their effect on the phase behavior of 2D anisotropic particles is very important. In a previous study we have shown that the inclusion of the exact third-virial coefficient in a density-functional theory dramatically changes the location of the phase transitions between different orientationally ordered phases [8]. The main effect of three-body correlations is a substantial decrease in the packing fraction of the I-T transition for all aspect ratios, which entails an enlarged region of tetratic phase stability [8]. The latter is an orientationally ordered phase with an orientational distribution function having fourfold symmetry: $f(\phi + n\pi/2) = f(\phi)\,(n = 1, \ldots, 4)$. In an analogous way, we expect the widening of the TR phase stability region in a HT fluid when the third-virial coefficient is incorporated into the theory. In particular, the packing fraction of the I-TR transition is expected to decrease, a result supported by MC simulations conducted on equilateral HT, where the transition was found at densities well below that estimated by SPT [34]. Recently a third-virial theory of freely rotating hard biaxial particles also resulted in being crucial to adequately predict the relative stability between orientationally ordered phases [42].

However, we believe the inclusion of nonuniform phases (such as the crystal phase) would be an essential feature of more systematic studies in the future. In this line, the recently derived fundamental-mixed-measure density-functional theory for hard, freely rotating 2D particles is at present the most promising theoretical tool to tackle this problem [2].

ACKNOWLEDGMENTS

Financial support under Grants No. FIS2015-66523-P and No. FIS2013-47350-C5-1-R from Ministerio de Economía, Industria y Competitividad (MINECO) of Spain is acknowledged.

APPENDIX: PROOF OF THE ABSENCE OF A POLAR N PHASE

As pointed out already, the excluded area is minimal when the main axes of the triangles are at a relative angle of π. This would in principle discard any polar nematic phase with most of the particles pointing along a given direction. Instead, the HT will point with equal probability along two equivalent directors differing in an angle of π. To prove this result, suppose that the orientational distribution function $f_q(\phi)$ had the form

$$f(\phi; q) = (1 - q)\tilde{f}(\phi) + q\,\tilde{f}(\pi - \phi), \tag{A1}$$

where q is the probability that a given particle is oriented with respect to the director pointing along the $\phi = \pi$ direction. Therefore the particle will be oriented with respect to a second director (pointing along the direction $\phi = 0$) with probability $(1 - q)$. The function $\tilde{f}(\phi)$ is an orientational distribution function which in principle could have the property $\tilde{f}(\phi) \neq \tilde{f}(\pi - \phi)$. Then the free-energy per particle (9) is easily obtained as

$$\varphi = \log y - 1 + \frac{1}{2\pi}\int_0^{2\pi} d\phi\,\Psi(\phi; q)\log\Psi(\phi; q) + \frac{y}{2}\left[\sum_{j\geqslant 0} s_{2j}(\tilde{f}_{2j})^2 + (1 - 2q)^2\sum_{j\geqslant 0} s_{2j+1}(\tilde{f}_{2j+1})^2\right], \tag{A2}$$

where $f(\phi; q) = (2\pi)^{-1}\Psi(\phi; q)$, while $\{\tilde{f}_n\}$ are the Fourier coefficients of $\tilde{f}(\phi)$. The derivative of φ with respect to q gives

$$S(q) \equiv \frac{\partial\varphi}{\partial q} = \frac{1}{2\pi}\int_0^{2\pi} d\phi\,\Delta\tilde{\Psi}(\phi)\log\Psi(\phi; q) - 2y(1 - 2q)\sum_{j\geqslant 1} s_{2j+1}(\tilde{f}_{2j+1})^2, \tag{A3}$$

where $\Delta\tilde{\Psi}(\phi) \equiv \tilde{\Psi}(\pi-\phi) - \tilde{\Psi}(\phi)$. $S(q)$ is a monotonically increasing function because

$$S'(q) = \frac{1}{2\pi}\int_0^{2\pi} d\phi \frac{[\Delta\tilde{\Psi}(\phi)]^2}{\Psi(\phi;q)} + 4y\sum_{j\geqslant 0} s_{2j+1}(\tilde{f}_{2j+1})^2 \geqslant 0, \tag{A4}$$

due to the positiveness of the odd coefficients: $s_{2j+1} > 0\,\forall j \geqslant 1$. Moreover, using the symmetries $\Delta\tilde{\Psi}(\phi) = -\Delta\tilde{\Psi}(\pi-\phi)$ and $\Psi(\phi,\frac{1}{2}) = \Psi(\pi-\phi;\frac{1}{2})$, it can be easily shown that $S(\frac{1}{2}) = 0$. Thus the value $q = 1/2$ is the only one that satisfies the equilibrium condition $\frac{\partial\varphi}{\partial q} = 0$. Due to the distribution function symmetry, $f(\phi,\frac{1}{2}) = f(\pi-\phi,\frac{1}{2})$, the odd Fourier coefficients of the expansion of $f(\phi,\frac{1}{2})$ are all equal to zero. We have shown numerically that this is the case by minimizing the free energy with respect to all the Fourier coefficients, resulting in $\{f_{2j+1} = 0\}\ \forall\ j \geqslant 0$. The main conclusion we can extract from the preceding analysis is that the main particle axes are oriented with equal probability with respect to two equivalent, antiparallel nematic directors.

[1] M. A. Bates and D. Frenkel, J. Chem. Phys. **112**, 10034 (2000).
[2] R. Wittmann, C. E. Sitta, F. Smallenburg, and H. Löwen, J. Chem. Phys. **147**, 134908 (2017).
[3] Y. Martínez-Ratón, E. Velasco, and L. Mederos, J. Chem. Phys. **122**, 064903 (2005).
[4] A. Díaz-De Armas and Y. Martínez-Ratón, Phys. Rev. E **95**, 052702 (2017).
[5] J. A. Cuesta and D. Frenkel, Phys. Rev. A **42**, 2126 (1990).
[6] G. Bautista-Carbajal and G. Odriozola, J. Chem. Phys. **140**, 204502 (2014).
[7] H. Schlacken, H. J. Mogel, and P. Schiller, Mol. Phys. **93**, 777 (1998).
[8] Y. Martínez-Ratón, E. Velasco, and L. Mederos, J. Chem. Phys. **125**, 014501 (2006).
[9] A. Donev, J. Burton, F. H. Stillinger, and S. Torquato, Phys. Rev. B **73**, 054109 (2006).
[10] D. A. Triplett and K. A. Fichthorn, Phys. Rev. E **77**, 011707 (2008).
[11] J. A. Anderson, J. Antonaglia, J. A. Millan, M. Engel, and S. C. Glotzer, Phys. Rev. X **7**, 021001 (2017).
[12] C. Avendaño and F. A. Escobedo, Soft Matter **8**, 4675 (2012).
[13] C. E. Sitta, F. Smallenburg, R. Wittowski, and H. Löwen, Phys. Chem. Chem. Phys. **20**, 5285 (2018).
[14] K. Zhao, C. Harrison, D. Huse, W. B. Russel, and P. M. Chaikin, Phys. Rev. E **76**, 040401 (2007).
[15] V. Narayan, N. Menon, and S. Ramaswamy, J. Stat. Mech. (2006) P01005.
[16] T. Müller, D. de las Heras, I. Rehberg, and K. Huang, Phys. Rev. E **91**, 062207 (2015).
[17] M. González-Pinto, F. Borondo, Y. Martínez-Ratón, and E. Velasco, Soft Matter **13**, 2571 (2017).
[18] L. Walsh and N. Menon, J. Stat. Mech. (2016) 083302.
[19] S. Varga, P. Gurin, J.-C. Armas-Pérez, and J. Quintana-H, J. Chem. Phys. **131**, 184901 (2009).
[20] P. Charbonneau and H. Stark, J. Chem. Phys. **143**, 114505 (2015).
[21] J. A. Martínez-González, S. Varga, P. Gurin, and J. Quintana-H, J. Mol. Liq. **185**, 26 (2013).
[22] D. de las Heras and E. Velasco, Soft Matter **10**, 1758 (2014).
[23] T. Geigenfeind, S. Rosenzweig, M. Schmidt, and D. de las Heras, J. Chem. Phys. **142**, 174701 (2015).
[24] A. H. Lewis, I. Garlea, J. Alvarado, O. J. Dammone, P. D. Howell, A. Majumdar, B. M. Mulder, M. P. Lettinga, G. H. Koenderink, and D. G. Aarts, Soft Matter **10**, 7865 (2014).
[25] M. González-Pinto, Y. Martínez-Ratón, and E. Velasco, Phys. Rev. E **88**, 032506 (2013).
[26] P. I. C. Teixeira, Liq. Cryst. **43**, 1526 (2016).
[27] Y. Martínez-Ratón, E. Velasco, and L. Mederos, Phys. Rev. E **72**, 031703 (2005).
[28] D. de las Heras, Y. Martínez-Ratón, and E. Velasco, Phys. Rev. E **76**, 031704 (2007).
[29] Y. Martínez-Ratón, Liq. Cryst. **38**, 697 (2011).
[30] J. Talbot, J. Chem. Phys. **106**, 4696 (1997).
[31] K. Zhao, R. Bruinsma, and T. G. Mason, Nat. Commun. **3**, 801 (2012).
[32] S. P. Carmichael and M. S. Shell, J. Chem. Phys. **139**, 164705 (2013).
[33] M. Benedict and J. F. Maguire, Phys. Rev. B **70**, 174112 (2004).
[34] A. P. Gantapara, W. Qi, and M. Dijkstra, Soft Matter **11**, 8684 (2015).
[35] R. van Roij and B. Mulder, J. Phys. II (France) **4**, 1763 (1994).
[36] Y. Martínez-Ratón and J. A. Cuesta, Phys. Rev. Lett. **89**, 185701 (2002).
[37] A. G. Vanakaras and D. J. Photinos, Mol. Cryst. Liq. Cryst. **299**, 65 (1997).
[38] P. J. Camp, M. P. Allen, P. G. Bolhuis, and D. Frenkel, J. Chem. Phys. **106**, 9270 (1997).
[39] A. G. Vanakaras, A. F. Tersis, and D. J. Photinos, Mol. Cryst. Liq. Cryst. **362**, 67 (2001).
[40] S. Varga, A. Galindo, and G. Jackson, Phys. Rev. E **66**, 011707 (2002); J. Chem. Phys. **117**, 10412 (2002).
[41] A. Galindo, A. J. Haslam, S. Varga, G. Jackson, A. G. Vanakaras, D. J. Photinos, and D. A. Dunmur, J. Chem. Phys. **119**, 5216 (2003).
[42] S. Dussi, N. Tasios, T. Drwenski, R. van Roij, and M. Dijkstra, Phys. Rev. Lett. **120**, 177801 (2018).